Extracellular Ca^{2+} ions reduce NMDA receptor conductance and gating

Bruce A. Maki[2] and Gabriela K. Popescu[1,2]

[1]Department of Biochemistry and [2]Neuroscience Program, School of Medicine and Biomedical Sciences, University at Buffalo, The State University of New York, Buffalo, NY 14214

Brief intracellular Ca^{2+} transients initiate signaling routines that direct cellular activities. Consequently, activation of Ca^{2+}-permeable neurotransmitter-gated channels can both depolarize and initiate remodeling of the postsynaptic cell. In particular, the Ca^{2+} transient produced by NMDA receptors is essential to normal synaptic physiology, drives the development and plasticity of excitatory central synapses, and also mediates glutamate excitotoxicity. The amplitude and time course of the Ca^{2+} signal depends on the receptor's conductance and gating kinetics; these properties are themselves influenced both directly and indirectly by fluctuations in the extracellular Ca^{2+} concentration. Here, we used electrophysiology and kinetic modeling to delineate the direct effects of extracellular Ca^{2+} on recombinant GluN1/GluN2A receptor conductance and gating. We report that, in addition to decreasing unitary conductance, Ca^{2+} also decreased channel open probability primarily by lengthening closed-channel periods. Using one-channel current recordings, we derive a kinetic model for GluN1/GluN2A receptors in physiological Ca^{2+} concentrations that accurately describes macroscopic channel behaviors. This model represents a practical instrument to probe the mechanisms that control the Ca^{2+} transients produced by NMDA receptors during both normal and aberrant synaptic signaling.

The Journal of General Physiology

INTRODUCTION

Ca^{2+} ions regulate countless biochemical processes, and their levels are therefore tightly controlled in live cells and organisms. In healthy individuals, the concentration of Ca^{2+} in blood serum is maintained within a narrow range (2.2–2.6 mM), and systemic deviations from these levels bring about a series of undesirable symptoms (Pearce and Thakker, 1997). In brain, however, extracellular Ca^{2+} levels oscillate locally on a fast (millisecond) timescale and can reach concentrations as low as 0.1 mM during normal synaptic transmission, with more prolonged global changes observed during seizures and after ischemia (Nicholson et al., 1977; Benninger et al., 1980; Heinemann and Pumain, 1980; Heinemann et al., 1986; Silver and Erecińska, 1990). Activity-dependent depletion of extracellular Ca^{2+} within the synaptic space is mediated by the opening of Ca^{2+}-permeable channels, including NMDA receptors (Rusakov and Fine, 2003). NMDA receptor-mediated Ca^{2+} influx triggers a broad range of cellular processes in the postsynaptic neuron, ranging from synaptic plasticity to excitotoxicity (Hardingham and Bading, 2010). Nevertheless, whether and how these fluctuations in extracellular Ca^{2+} levels alter the amplitude and time course of the NMDA receptor-mediated flux remains unclear.

NMDA receptors generate significant Ca^{2+} transients as a result of their characteristically long activations and large unitary currents, of which a substantial fraction (~10–20%) is carried by Ca^{2+} (Burnashev et al., 1995). They are ligand-gated excitatory channels that require for activation the binding of both glutamate and the co-agonist glycine. Functional receptors assemble from two obligatory GluN1 subunits, which are ubiquitously expressed throughout the central nervous system, and two GluN2 or GluN3 subunits, of which GluN2A is the most prominently expressed subunit in adult brain and spinal cord (Monyer et al., 1994). Each subunit has a large extracellular portion that is organized into two globular modules: the N-terminal domain and the agonist-binding domain, of which the latter connects directly with the pore-forming transmembrane domain (Karakas and Furukawa, 2014; Lee et al., 2014). The transmembrane domain is composed of three transmembrane helices and a loop-helix segment that only partially penetrates the membrane from the cytoplasmic side (Burnashev et al., 1992; Wo and Oswald, 1995; Kuner et al., 1996). Lastly, the intracellular domain consists mainly of the C-terminal domain, which contains binding sites for Ca^{2+}-dependent proteins and residues that can be covalently modified by Ca^{2+}-dependent enzymes (Chen and Roche, 2007; Choi et al., 2011).

GluN1/GluN2A responses are modulated directly by numerous physiological ligands, including inorganic

Correspondence to Gabriela K. Popescu: popescu@buffalo.edu

Abbreviations used in this paper: LL, log likelihood; RT, rise time.

The Rockefeller University Press $30.00
J. Gen. Physiol. Vol. 144 No. 5 379–392
www.jgp.org/cgi/doi/10.1085/jgp.201411244

cations. At low nanomolar concentrations, H^+ and Zn^{2+} interact with sites on the N-terminal domain and reduce currents with voltage-independent allosteric mechanisms (Tang et al., 1990; Traynelis and Cull-Candy, 1990; Paoletti et al., 1997; Banke et al., 2005; Erreger and Traynelis, 2008; Amico-Ruvio et al., 2011). In contrast, at micromolar concentrations, Zn^{2+} and Mg^{2+} bind within the membrane pore and obstruct the passage of permeant ions with voltage-dependent blocking mechanisms (Mayer et al., 1984; Nowak et al., 1984; Christine and Choi, 1990; Legendre and Westbrook, 1990). Extracellular Ca^{2+} reduces NMDA receptor unitary conductance in a concentration-dependent but voltage-independent manner (Ascher and Nowak, 1988) distinct from the flickering block induced by Mg^{2+} (Nowak et al., 1984). However, a hypothesis that is still in circulation proposes that the Ca^{2+}-dependent decrease in channel conductance also reflects a blocking mechanism. Despite this, because this "Ca^{2+} block" is voltage independent, the responsible Ca^{2+}-binding site most likely resides outside of the membrane field, and under physiological conditions, its occupancy appears to be submaximal (K_d = ~0.9 mM; Premkumar and Auerbach, 1996; Sharma and Stevens, 1996). Recent studies suggest that the site responsible for Ca^{2+} block resides along the GluN1 subunit just external to the channel gate (Watanabe et al., 2002; Karakas and Furukawa, 2014); however, whether this or other direct interactions between Ca^{2+} and receptor residues influence channel gating remains unclear.

In addition to the effect of external Ca^{2+} ions on conductance, several internal Ca^{2+}-activated proteins interact with the C-terminal domain of the NMDA receptor and modify receptor gating properties over a broad timescale (Tong et al., 1995; Zhang et al., 1998; Krupp et al., 1999, 2002; Rycroft and Gibb, 2004a,b). This additional layer of Ca^{2+}-dependent effects has constrained the majority of NMDA receptor reaction mechanisms to ionic conditions with unphysiologically low or absent external Ca^{2+} levels (Popescu et al., 2004; Erreger et al., 2005; Dravid et al., 2008; Vance et al., 2013). In the few instances when reaction mechanisms have been investigated in physiological [Ca^{2+}], potential gating differences between Ca^{2+}-bound and Ca^{2+}-free receptors were not addressed (Lester and Jahr, 1992; Banke and Traynelis, 2003; Schorge et al., 2005).

We used kinetic analyses and modeling of single-channel data obtained over a range of external Ca^{2+} concentrations to develop a comprehensive view of the direct effects of Ca^{2+} on NMDA receptor conductance and gating. We found that external Ca^{2+} reduced both the channel unitary conductance and the receptor gating kinetics with half-maximal effects occurring within the physiological range of $[Ca^{2+}]_e$. We report a kinetic model that incorporates both of these effects and thus can be used to predict and explain the amplitude and time course of NMDA receptor macroscopic responses during dynamic fluctuations in $[Ca^{2+}]_e$. This new knowledge will assist future efforts to delineate the roles of NMDA receptor signals in health and disease.

MATERIALS AND METHODS

Cells and receptor expression

HEK293 cells (ATCC number CRL-1573 at passages 22–32) were maintained in Dulbecco's modified Eagle's medium (DMEM) supplemented with 10% fetal bovine serum and 1% penicillin/streptomycin. Cells were transiently transfected with the Ca^{2+} phosphate method (Chen and Okayama, 1987; Kussius et al., 2009) using pcDNA3.1 (+) plasmids expressing rat GluN1-1a (P35439-1), rat GluN2A (Q00959), and GFP using a total of ~3 µg DNA in a 1:1:1 ratio. Proteins lacking intracellular domains were expressed from constructs encoding stop codons at residues K838 in GluN1-1a and K844 in GluN2A (Krupp et al., 1999, 2002). Cells were incubated with transfection mixture for 2 h, after which they were washed twice with PBS and allowed to recover in growth medium supplemented with 2 mM $MgCl_2$. Cells were used for electrophysiological measurements 24–48 h later.

Electrophysiology

Whole-cell currents were recorded with borosilicate glass pipettes (2–5 MΩ) filled with intracellular solution containing (mM) 135 CsCl, 33 CsOH, 2 $MgCl_2$, 11 EGTA, 1 $CaCl_2$, and 10 HEPES, adjusted to pH 7.4 (CsOH). Cells were held at −70 mV, unless indicated otherwise, and were perfused with extracellular (wash) solutions containing (mM) 150 NaCl, 2.5 KCl, 0.01 EDTA, 10 tricine, 0.1 glycine, and 10 HEPBS (*N*-(2-Hydroxyethyl)piperazine-*N*′-(4-butanesulfonic acid)), adjusted to pH 8.0 (NaOH), some of which were supplemented with 1 mM glutamate and/or $CaCl_2$ concentrations as indicated. For each condition, currents were recorded for 5 s, with or without 5-s wash periods between protocols, as indicated. For each cell, 5–10 runs were recorded sequentially and traces were averaged. Currents were amplified and filtered (2 kHz, Axopatch 200b) and then sampled (5 kHz, Digidata 1440A) into digital files (pCLAMP software; Molecular Devices) and stored. For each cell, the amplitude of the peak current (I_{pk}) was measured directly from the mean trace, and the amplitude of the steady-state current (I_{ss}) was determined from fitting a single exponential function to the decaying phase of the trace (as indicated in Fig. 1 A). The inhibitory effect of $[Ca^{2+}]_e$-dependent inhibition was monitored by determining the ratio of the steady-state current measured with Ca^{2+} (I_{Ca}) to that of the steady-state current measured initially in the absence of Ca^{2+} (I_{ss}), and the maximum inhibitory effects and half-maximal inhibitory concentrations (IC_{50}) were calculated by fitting the Hill equation to the data. The percent inhibition across $[Ca^{2+}]_e$ was expressed as $(1 - I_{Ca}/I_{ss}) \times 100$.

Unitary currents were recorded from outside-out excised patches using borosilicate glass pipettes (15–25 MΩ) filled with the intracellular solution described above for whole-cell recordings. Patches containing one to five receptors were perfused with Na^+-containing external solutions composed of (mM) 150 NaCl, 2.5 KCl, 10 HEPBS, 10 tricine, 1 glutamate, and 0.1 glycine, adjusted to pH 8.0 (NaOH) and supplemented sequentially with 0, 0.5, 1.8, 5, or 10 mM $CaCl_2$, followed by a Ca^{2+}-only solution composed of (mM) 75 $CaCl_2$, 2.5 KCl, 10 HEPBS, 10 tricine, 1 glutamate, and 0.1 glycine, adjusted to pH 8.0 (Tris-OH). Patches were first exposed to the Ca^{2+}-free solution and held at membrane potentials ranging from −100 to 20 mV, varied step-wise in 10-mV increments. At each holding potential, the currents were recorded for several seconds, so that the record contained a sufficient fraction of

unitary currents to allow accurate determination of the unitary current amplitude, and the protocol was repeated using extracellular solutions of increasing [Ca^{2+}]. Data were amplified and filtered (2 kHz, Axopatch 200B), sampled (5 kHz, Digidata 1400A), and digitally stored using pCLAMP software. Within each experimental condition, segments containing runs of openings to a single amplitude level were selected for analyses, and the remaining periods, which often included openings to two or more amplitude levels, were discarded. Data were processed and analyzed using QuB software. After digitally filtering (12 kHz) the record, unitary current amplitudes (i) were estimated statistically with the SKM algorithm while imposing no dead time (Qin, 2004). For each [Ca^{2+}] and amplitude level, the unitary conductance (γ) and the unitary reversal potential (E_{rev}) were computed as the slope and intercept, respectively, of a linear fit to the i/V data. The Ca^{2+}-dependent inhibition at each [Ca^{2+}] for both principal (P) and secondary (S) conductance levels were determined as the ratio of the mean conductance relative to that measured in 0 and 1.8 mM Ca^{2+}, respectively (γ/γ_{max}). Maximal inhibitory effects and IC_{50} were calculated by fitting the Hill equation to the data.

Macroscopic responses to brief (10 ms) agonist exposures were recorded from outside-out excised patches with borosilicate glass pipettes (5–15 MΩ) filled with the internal solution described above for whole-cell measurements. External solutions were exchanged by moving the patch rapidly with a piezo translation system (Burleigh LSS-3100/3200) across the interface formed by wash and agonist-containing solutions from a double-barrel theta-glass tube (Amico-Ruvio et al., 2011). Only current traces exhibiting 10–90% solution exchange time between 0.15 and 0.25 ms, as measured by open tip potentials immediately after the experiment, were used for analysis. Currents were amplified and filtered (Axopatch 200b) and then sampled and digitally stored with pCLAMP software. I_{pk} and the 10–90% rise time (RT) of the current were measured directly from the trace mean, and the kinetics of current decay upon removing glutamate were determined by fitting a double exponential function to the declining phase of the mean trace, with each component having a corresponding time constant (τ_{slow} and τ_{fast}) and area (A_{slow} and A_{fast}). The weighted time constant of decay (τ_w) was calculated according to the equation $\tau_w = \tau_{slow}(A_{slow}/(A_{slow} + A_{fast})) + \tau_{fast}(A_{fast}/(A_{slow} + A_{fast}))$.

Stationary one-channel activity was recorded with the patch-clamp technique from cell-attached patches. Fire-polished borosilicate glass pipettes (15–25 MΩ) were filled with extracellular solutions containing (mM) 150 NaCl, 2.5 KCl, 10 HEPBS, 10 tricine, 1 glutamate, and 0.1 glycine, adjusted to pH 8.0 (NaOH), and were supplemented with 0, 1.8, or 5 $CaCl_2$, as indicated. Currents were driven inward by applying a pipette potential of 40 mV (E_m, approximately −50 mV), where voltage-dependent block by contaminating Mg^{2+} ions is negligible (Mayer et al., 1984; Nowak et al., 1984). In addition, currents were recorded with extracellular solution containing (mM) 75 $CaCl_2$, 2.5 KCl, 10 HEPBS, 10 tricine, 1 glutamate, and 0.1 glycine, adjusted to pH 8.0 (Tris-OH). To resolve openings in Ca^{2+}-only solutions, where current amplitudes are much smaller but Mg^{2+} block is largely relieved (Mayer and Westbrook, 1987), currents were recorded with 100-mV pipette potentials (E_m, approximately −110 mV). These data were compared with controls obtained also at 100 mV but in Ca^{2+}- and Mg^{2+}-free solutions (1 mM EDTA). Currents were amplified and filtered (10 kHz; Axopatch 200B), sampled (40 kHz; National Instruments PCI-6229 A/D Board), and stored into digital files (QuB software; SUNY Buffalo).

Kinetic analyses were performed on files with low-noise baseline (peak-to-peak <1 pA, RMS = 0.2–0.3 pA) and containing a sufficient number of events (>10,000 events, >10 min recording time) to increase the likelihood of observing double openings if more than one channel was present in the patch. Data were processed and idealized as described above for excised patches. To these idealized data, kinetic models containing two or three conductance classes, depending on the presence or absence of the S conductance level, were fit directly with the MIL algorithm in QuB while imposing a dead time of 0.075 ms (three samples; Qin et al., 1997). Individual closed (C) and open (O_P or O_S) states were sequentially added as necessary to increase the goodness of fit, which was evaluated by monitoring the maximum value of the log likelihood (LL) function. A threshold of 10 LL units per added state was imposed to determine best fit, and the model obtained was used to extract global kinetic parameters, time constants (τ, ms), and areas (a, %) for individual closed (E_1–E_5) and open (E_F, E_L, E_M, and E_H) exponential components and to estimate rate constants (s^{-1}) for all explicit transitions in the model. Maximal inhibitory effect and IC_{50} were calculated by fitting the Hill equation to the measured dependence of the open probability (P_o) on [Ca^{2+}].

For low P_o files, even if no double openings are apparent within any one burst, the possibility still exists that consecutive bursts originate from separate receptors, thus introducing an error in rate estimations. We tested for this possibility in two ways. First, we calculated the likelihood that the recorded currents originated from two or more alternately open channels by determining the number of bursts in an individual file and the proportion of bursting activity in that file, as previously described (Colquhoun and Hawkes, 1995). We defined bursts as groups of openings that were separated by closed events shorter than a τ_{crit}, which was calculated to exclude events pertaining to E4 and E5 components, and misclassified the same number of E_3 and E_4 events (Magleby and Pallotta, 1983). With this method, we determined that for all files used in our analyses the likelihood that all bursts originated from the same channel was >95%. For example, for the shortest record used (10 min; P_o, 0.06; 1.7×10^4 events), we observed 70 bursts that represented 8% of the recorded time, thus indicating a 95.6% chance that all bursts were produced by the same channel. As a second test, we used the model deduced for 75 mM Ca^{2+} (see Fig. 6, bottom arm) and simulated 10 min of data from one channel. We then refitted our model to this simulated data assuming the trace was produced by two channels. With this assumption, only one rate changed: the recovery from the longest lived closed state, which is the primary state that produces gaps between bursts, was approximately threefold slower (0.2 s^{-1} vs. 0.06 s^{-1}). This result was replicated for the model and rates obtained with 1.8 mM Ca^2; the only rate that changed by assuming two channels in the patch was the recovery rate from the longest lived closed state (0.2 s^{-1} vs. 0.08 s^{-1}). However, the model with this much slower recovery rate predicted macroscopic responses with I_{ss}/I_{pk} = 0.15; this disagrees with the whole-cell measurement, for which I_{ss}/I_{pk} = 0.40 (see Fig. 1 B). Based on these tests, we conclude that in the records we selected for analyses all of the bursts most likely originated from a singular channel.

Free energy profiles were calculated and illustrated relative to the free energy of their respective C_3 closed state, which represents the first fully liganded state along the glutamate-initiated activation reaction. Calculations were performed using the measured rate constants in each model according to the relationship $\Delta G^0 = -RT(\ln K_{eq})$, where R represents the molar gas constant, T represents the absolute temperature, and K_{eq} represents the equilibrium constant for the indicated transition calculated as the ratio of the forward and reverse reactions (k_+/k_-). Barrier heights ($E^{\ddagger}$) were calculated according to the relationship $E^{\ddagger} = \Delta G^0 + (10 - \ln k_+)$. Individual peaks and wells were arbitrarily equally spaced along the reaction coordinate.

Simulations

Ensemble currents through 100 receptors were simulated using the experimentally determined unitary conductance and the tiered kinetic model in Fig. 6 A. Two identical glutamate-binding steps

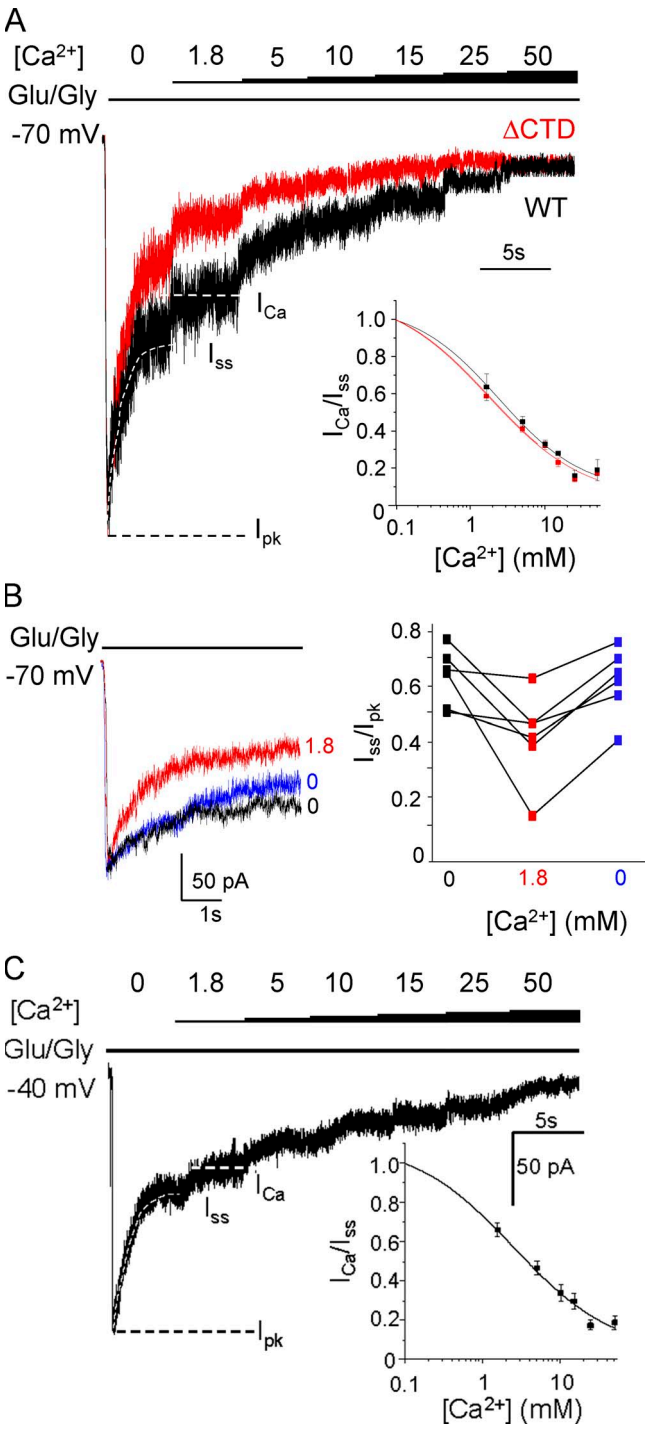

Figure 1. [Ca^{2+}]-dependent inhibition of macroscopic GluN1/GluN2A responses. (A) Representative whole-cell currents recorded from WT receptors (black) and receptors lacking the intracellular C-terminal tails (ΔCTD, red) at increasing concentrations of extracellular Ca^{2+} are illustrated normalized to I_{pk}. (inset) Dose dependency of steady-state inhibition. (B, left) Representative whole-cell currents recorded from WT receptors before (0, black) and after applying (red) 1.8 mM Ca^{2+}, and subsequently after removing Ca^{2+} (0, blue). (right) Summary of changes in macroscopic desensitization expressed as I_{ss}/I_{pk} ratio. (C) Representative whole-cell currents recorded from WT receptors at −40 mV. (inset) Dose dependency of steady-state current. Error bars indicate SEM.

were appended to the C_3 state in each model using association and dissociation rate constants measured previously (1.7×10^7 $M^{-1}s^{-1}$ and 60 s^{-1}, respectively; Popescu et al., 2004), and all receptors were placed initially at the resting, unliganded state. Responses to phasic (10 ms) and tonic (5 s) stimuli were calculated as the time-dependent accumulation of receptors into the open state or states upon exposure to 1 mM glutamate. Simulated responses were processed and analyzed as described for the experimentally recorded currents.

Statistics

All results are presented as means with the associated standard errors (SEM). Statistical significance of differences were evaluated with the paired *t* test for data obtained from the same cell and with the unpaired *t* test for data obtained from separate cells, as indicated. Differences were considered significant for $P < 0.05$.

RESULTS

Fast reversible inhibition of macroscopic responses by external [Ca^{2+}]

To examine the concentration-dependent effects of external Ca^{2+} on macroscopic NMDA receptor currents, we recorded whole-cell responses from HEK293 cells transiently expressing recombinant rat GluN1/GluN2A receptors. Currents were elicited in the absence of Ca^{2+} (1 mM EDTA) with suprasaturating concentrations of glutamate (1 mM, EC_{50} = 3 µM; Popescu et al., 2004) and glycine (0.1 mM, EC_{50} <1 µM; Johnson and Ascher, 1987; Kleckner and Dingledine, 1988) and were allowed to equilibrate for 5 s before applying increasing concentrations of Ca^{2+}. We observed a rapid and concentration-dependent reduction in the steady-state current level (I_{Ca}) relative to the initial plateau obtained in 0 mM Ca^{2+} (I_{ss}), which for 1.8 mM Ca^{2+} was 40 ± 10% (calculated as $(1 - I_{Ca}/I_{ss}) \times 100$; Fig. 1 A). In the 0–50-mM range tested, the Hill equation predicted a maximum fractional inhibition of 92 ± 9% and a half-maximal dose (IC_{50}) of 2.4 ± 0.7 mM (n = 5; Fig. 1 A, inset). From the fast onset of the observed inhibition and its rapid and complete reversibility (Fig. 1 B), we inferred that it arose from direct interactions between Ca^{2+} ions and channel residues rather than through indirect, second-messenger effects of Ca^{2+}, whose kinetics are slower.

To test this inference directly, we examined responses from NMDA receptors that lacked the C-terminal tails of both GluN1 and GluN2A subunits (ΔCTD). These receptors have altered gating kinetics and produce macroscopic responses that desensitize faster and deeper (Maki et al., 2012). Despite a reduced response in 0 mM Ca^{2+} (I_{ss}), neither the extent of inhibition (94 ± 12%) nor the IC_{50} (1.8 ± 0.7 mM) were significantly different relative to full-length receptors (n = 7, $P > 0.05$, unpaired *t* test; Fig. 1 A). This result demonstrates that the observed [Ca^{2+}]-dependent inhibition of the NMDA receptor response was independent of intracellular

receptor domains and thus it was likely mediated by external or permeating Ca^{2+} ions.

To distinguish whether current inhibition occurred via interactions between Ca^{2+} ions in the bulk solution with the receptor's extracellular domains or between permeating Ca^{2+} with residues along the transmembrane pore, we recorded responses at a depolarized holding potential (−40 mV), where binding to residues within the pore would be reduced (Woodhull, 1973). We found that the extent of inhibition and IC_{50} values were not statistically different from those measured at −70 mV (96 ± 13% and 2.5 ± 0.9 mM, respectively; $n = 5$, $P > 0.05$, unpaired t test; Fig. 1 C), thus confirming previous reports that the inhibitory effect of Ca^{2+} on NMDA receptor currents is voltage independent (Premkumar and Auerbach, 1996; Sharma and Stevens, 1996).

Together, these results indicate that Ca^{2+} ions inhibit NMDA receptor current fluxes through direct interactions with extracellular receptor residues. The observed reduction in macroscopic current may reflect a decrease in the number of channels present, their unitary conductance (γ), and/or their gating kinetics (P_o). Given that the inhibition of whole-cell currents was rapid and fully reversible, we conclude that the number of channels assayed did not change over the course of our measurements; therefore, we examined next the effects of external [Ca^{2+}] on unitary channel properties.

Direct effects of external [Ca^{2+}] on unitary conductance and permeability

We first examined the [Ca^{2+}]-dependent effects on unitary conductance by measuring unitary current amplitudes (i) at several membrane voltages in excised patches. This configuration allowed us to control and vary both the extracellular [Ca^{2+}] (0–75 mM) and the membrane potential (−100 to 20 mV), while recording activity continuously from the same small channel population (Fig. 2 A). Consistent with literature reports, we found that, relative to Na^+-only currents (i_{Na}), adding Ca^{2+} in the extracellular solution produced two observable effects on the unitary current amplitude (Ascher and Nowak, 1988; Jahr and Stevens, 1993). First, its mean level decreased with increasing [Ca^{2+}] ($i < i_{Na}$), and second, in addition to a principal conductance level (P), a secondary conductance level (S) developed (Fig. 2 A). For each [Ca^{2+}] we calculated the unitary conductance (γ) as the slope of linear regressions to the i/V data (Fig. 2 B) and found that this was as follows: γ_{Na}, 62.7 ± 0.7 pS in 0 mM Ca^{2+}; γ_P, 53 ± 5 pS and γ_S, 37 ± 4 pS in physiological [Ca^{2+}] (1.8 mM); and γ_P, 18.1 ± 0.5 pS and γ_s, 9.8 ± 0.8 pS when Ca^{2+} was the only permeant ion (75 mM). The Hill equation estimated the maximum effect on γ_P, 76 ± 4% and the IC_{50}, 6.3 ± 0.8 mM; and on γ_S, 74 ± 2%; and the IC_{50}, 6.4 ± 1.0 (Fig. 2 C).

Similar [Ca^{2+}]-dependent reductions in NMDA receptor conductance have been measured in several native preparations (Ascher and Nowak, 1988; Jahr and Stevens, 1993), and this is believed to be a conserved property across GluN1/GluN2 isoforms. In the current literature, the phenomenon is referred to as "Ca^{2+}-block," although a blocking mechanism has not yet been demonstrated and clearly the Ca^{2+}-binding site or sites responsible for this effect lie externally to the membrane field (Ascher and Nowak, 1988; Jahr and Stevens, 1993). Similarly, the mechanism by which the two conductance levels arise is unknown. Our result indicated that γ_S and γ_P had similar IC_{50} values ($P > 0.5$, paired t test) but distinct Hill coefficients: 1.1 ± 0.2 and 2.5 ± 0.2 mM, respectively ($P < 0.05$, paired t test). This observation may indicate that two or more Ca^{2+}-binding sites of similar affinities

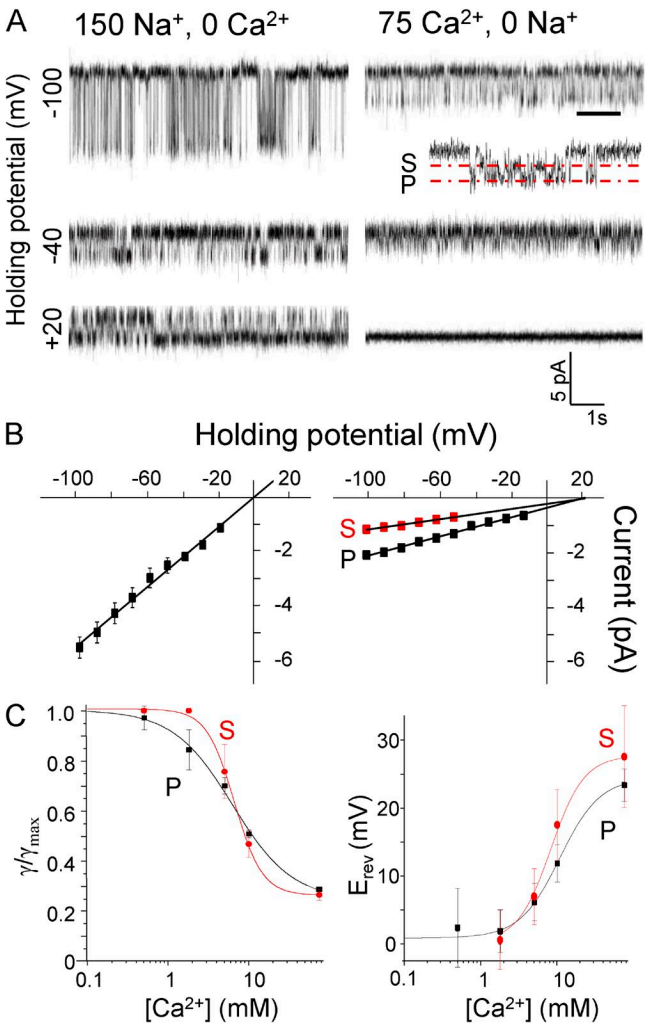

Figure 2. Ca^{2+} effects on GluN1/GluN2A receptor unitary conductance. (A) Representative Na^+-only (left) or Ca^{2+}-only (right) unitary currents recorded at three membrane potentials from the same receptor (outside-out excised patch; open is down at negative potentials). In Ca^{2+}-only, two unitary current levels are apparent: principal (P) and secondary (S). (B) Current-voltage relationships for the P and S current levels. (C) Concentration dependence of unitary conductance and reversal potentials for P and S conductance levels. Error bars indicate SEM.

may be coupled when the channel exists in the S level conformations but not the P level conformations.

Because in Na^+-only solutions a second conductance is not apparent, the presence of two conductance levels in Ca^{2+}-containing solutions may be explained in two ways. One possibility is that regardless of external [Ca^{2+}], the pore may exist in two structural conformations, corresponding to P and S, which have similar Na^+ but distinct Ca^{2+} permeabilities, such that higher Ca^{2+} permeation will result in lower conductance. In other words, the presence of Ca^{2+} may reveal rather than produce the lower conductance conformation. Alternatively, a separate pore conformation that is rarely visited when only Na^+ is present may be substantially stabilized by Ca^{2+} binding. To distinguish between these two possibilities, we examined the relative Ca^{2+} permeabilities of the P and S conductance levels.

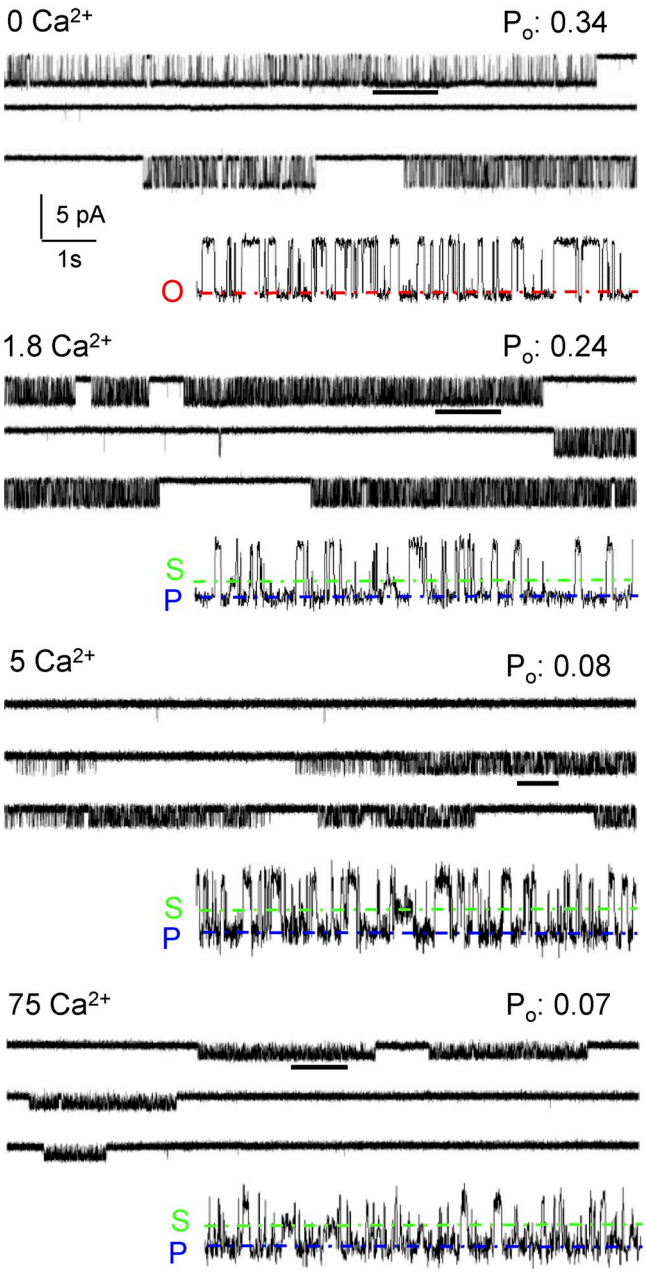

Figure 3. Ca^{2+} effects on GluN1/GluN2A gating. Representative current traces recorded from cell-attached patches containing one active receptor with the indicated pipette [Ca^{2+}] (mM). P_o values listed are means calculated for the entire record from which the displayed trace was selected. Underlined portions of traces are magnified below to different degrees to highlight the salient changes.

As an index of relative Ca^{2+} permeability, we measured the extent to which the reversal potentials (E_{rev}) for each conductance level shifted when switching from Na^+-only to Ca^{2+}-only solutions. We calculated E_{rev} as the zero current intercept of extrapolated linear regressions to i/V data (Fig. 2 B) and found that the shift in E_{rev} was similar for both P and S levels: 24 ± 2 and 28 ± 5 mV, respectively ($P > 0.05$, paired t test; Fig. 2 C), corresponding to a relative Ca^{2+} permeability (P_{Ca}/P_{Na}) of ∼7–8 for each. This result indicates that the proportional composition of passed current is largely similar for both P and S, and thus, the secondary level does not arise from increased Ca^{2+} permeation, ruling out the first scenario.

Together, these results show that Ca^{2+} binding (IC_{50}, ∼6 mM) to one or more external sites can decrease the unitary NMDA receptor conductance as much as approximately threefold. Ca^{2+} binding may stabilize receptors into a state of even lower conductance (S), which is not significantly populated in Na^+-only solutions, and may be indicative of a receptor conformation in which Ca^{2+}-binding sites are coupled. Importantly, despite the lower conductance of S compared with P, both have similar P_{Ca}/P_{Na}. Based on these results, we estimate that physiological Ca^{2+} (1.8 mM) will decrease GluN1/GluN2A conductance by ∼10 pS, or 15%, relative to Na^+-only solutions. Whereas this decrease is substantial, it does not fully account for the 40% inhibition observed in whole-cell currents (calculated as $(1 - I_{Ca}/I_{ss}) \times 100$; Fig. 1 A). Therefore, we inferred that the difference may reflect slower gating of Ca^{2+}-bound GluN1/GluN2A receptors. Next, we investigated this possibility by examining direct effects of external [Ca^{2+}] on channel gating.

Direct effects of external [Ca^{2+}] on gating kinetics

Using cell-attached patches containing one GluN1/GluN2A receptor, we recorded uninterrupted steady-state activity for long (>10 min) periods. As described for excised patches above, increasing external [Ca^{2+}] produced two resolvable amplitude levels, P and S, indicative of two distinct open states, O_P and O_S, respectively (Fig. 3). As a measure of overall channel activity, we estimated the channel closed probability (P_C) and calculated an aggregated open probability containing events at both open conductance levels as $P_o = 1 - P_C$. We found that, indeed, the aggregated P_o decreased with increasing [Ca^{2+}] from 0.38 ± 0.08 in 0 mM Ca^{2+} to in 0.27 ± 0.03 in 1.8 mM Ca^{2+}, corresponding to a ∼30%

reduction in channel activity under physiological conditions. A fit with the Hill equation to the dose dependency of P_o across the range of [Ca^{2+}] predicted a 65 ± 4% maximum inhibition and IC_{50} = 1.7 ± 0.2 mM (Fig. 3 and Table 1).

Single-channel observations allow the direct measurement of dwell durations in each conductance level. We measured the mean duration of openings (MOT) as the aggregated durations for O_P and O_S and found that this was not different across [Ca^{2+}], indicating that the observed reduction in P_o was caused entirely by a lengthening of closed intervals. Indeed, the mean closed time (MCT) increased progressively by ∼6- and ∼17-fold in 5 and 75 mM Ca^{2+}, respectively (Fig. 3 and Table 1). When we segregated events measured for the O_P and O_S, we found that relative to O_P, O_S events were much less frequent such that the aggregated P_o was very similar to the overall probability of O_P openings (Fig. 3 and Table 1). Relative to 1.8 mM Ca^{2+}, in Ca^{2+} only, the mean duration of O_S events increased slightly (from 2.6 to 3.5 ms) and its fractional area increased ∼3-fold; however, even in Ca^{2+} only, the occupancy of O_S remained >10-fold lower than that of O_P. Combined with the relatively small difference in conductance between S and P, we conclude that quantitatively, the [Ca^{2+}]-dependent reduction in channel conductance by the appearance of O_S is negligible. Importantly, the observation that the channel MOT was relatively constant across Ca^{2+} concentrations, whereas the MCT was substantially increased, argues against a classic open-block mechanism as the explanation for the decrease in conductance (Neher and Steinbach, 1978). Instead, an allosteric mechanism appears more plausible.

Next, we examined the duration of dwells observed in closed (C) and open (O_S and O_P) states. It is well established that, in the absence of Ca^{2+}, GluN1/GluN2A receptors produce closed duration distributions that can be reliably described with five exponential components (E_1–E_5; Kussius et al., 2009). The faster components (E_1–E_3) occur within activation bursts, and the two slowest components (E_4 and E_5) represent dwells in desensitized states, which terminate bursts. We found that with increasing external [Ca^{2+}], the number of closed components remained unchanged; however, their time constants were gradually increased (Fig. 4 and Table 2). In addition, the fraction of very short (E_1) and very long (E_5) events increased, mostly at the expense of E_3 events.

The distribution of openings changed in a different manner. In the absence of external Ca^{2+}, GluN1/GluN2A receptors open to a uniform amplitude level with two kinetic components (Popescu and Auerbach, 2003). Shifts between low, medium, and high P_o gating modes cause the longer open component to change duration (E_L, E_M, or E_H), whereas the fast component (E_F) remains unchanged. Therefore, long recordings in which all three modes are sampled contain up to four open components: E_F, E_L, E_M, and E_H. The distribution of receptors across gating modes determines the shape of synaptic current; therefore, it is important to examine whether modal gating persists when Ca^{2+} is present and whether it is apparent for both O_P and O_S. We found that O_P had a kinetic distribution that very closely resembled the behavior of open states in 0 mM Ca^{2+} (O). Thus, in 1.8 mM Ca^{2+} we resolved four kinetic components whose time constants were not statistically different from E_F, E_L, E_M, and E_H in 0 mM Ca^{2+} (Fig. 4 and Table 3). However, increasing external [Ca^{2+}] increased the prevalence of the medium mode (a_{EM}) from 34% in 0 mM Ca^{2+} to 48, 58, and 77% in 1.8, 5, and 75 mM Ca^{2+}, respectively. This increase occurred at the expense of the low P_o mode, such that the shorter openings (E_L) were observed in only one recording in 5 mM Ca^{2+} and were absent in 75 mM Ca^{2+}. Therefore, the O_P state behaved kinetically in a manner similar to the singular O state observed in 0 mM Ca^{2+}, and Ca^{2+} binding to an external site may favor openings in the medium mode, by an allosteric effect. In contrast, openings in O_S were kinetically homogeneous across concentrations, being consistently well described with one exponential whose lifetime was slightly increased in 75 mM Ca^{2+}. This observation is consistent with the hypothesis that O_S represents a new conformation that is stabilized specifically by Ca^{2+} binding to an external site.

Kinetic models describing modulation of NMDA receptor responses by external Ca^{2+}

We attempted to capture the [Ca^{2+}]-dependent changes in conductance and gating into one comprehensive

TABLE 1

Effects of external [Ca^{2+}] on single-channel kinetics

[Ca^{2+}]	P_o		P_o (1 − P_{closed})	MCT	MOT		Events
	O_P	O_S			O_P	O_S	
mM				*ms*	*ms*	*ms*	
0 (*n* = 7)	0.38 ± 0.08	-	0.38 ± 0.08	12 ± 4	5.0 ± 0.6	-	1.6×10^6
1.8 (*n* = 5)	0.26 ± 0.04	0.006 ± 0.001	0.27 ± 0.03	16 ± 4	4.9 ± 0.6	2.6 ± 0.4	1.9×10^6
5 (*n* = 6)	0.13 ± 0.06[a]	0.007 ± 0.003	0.14 ± 0.06[a]	70 ± 30[a]	4.0 ± 0.7	2.8 ± 0.7	3.4×10^5
75 (*n* = 7)	0.18 ± 0.06[a]	0.02 ± 0.01[a]	0.20 ± 0.07	200 ± 100[a]	6.4 ± 0.7	3.5 ± 0.3[a]	2.3×10^5

[a]$P < 0.05$ relative to 0 mM Ca^{2+} for O_P and relative to 1.8 mM Ca^{2+} for O_S (unpaired *t* test).

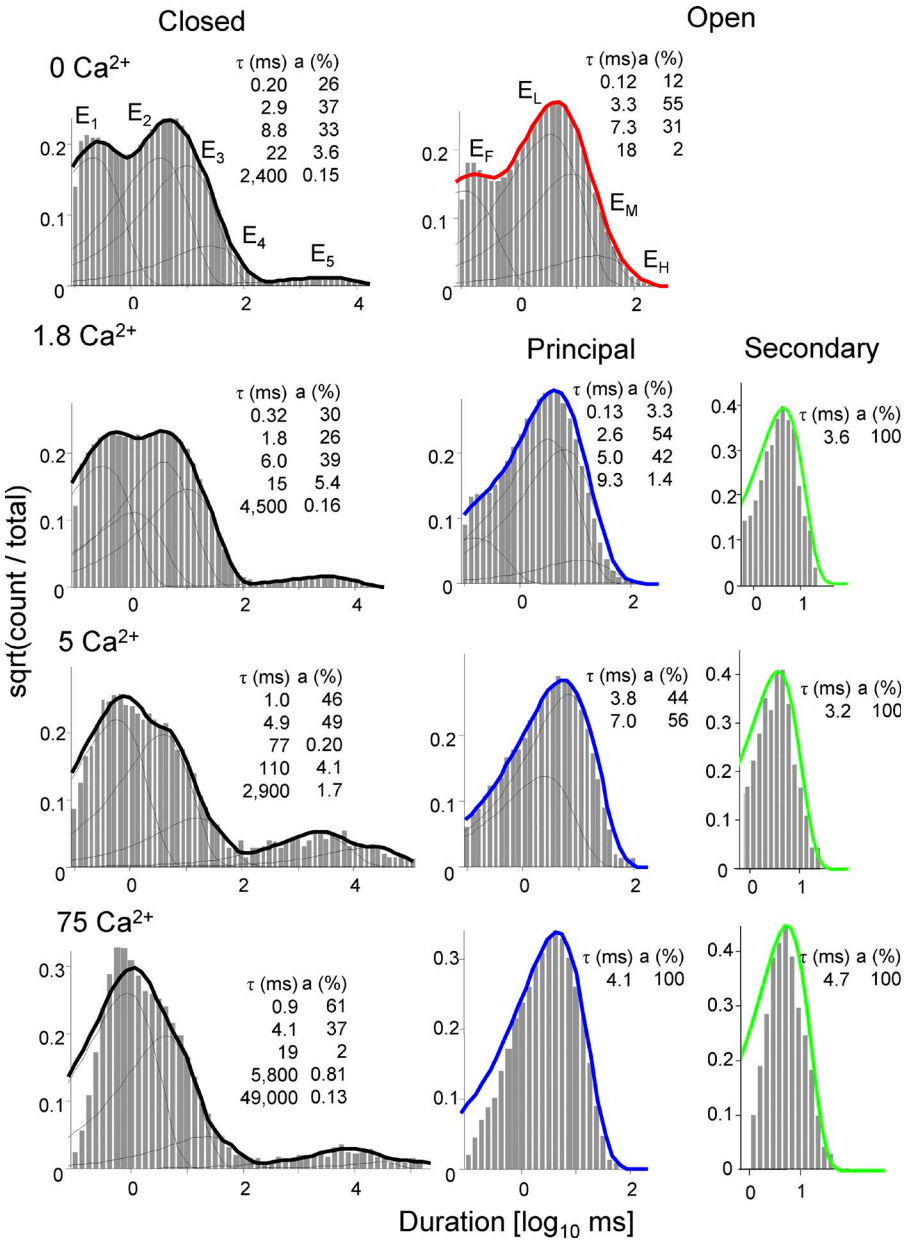

Figure 4. Ca^{2+} effects on closed and open event distributions. Closed (left) and open (middle and right) intervals observed in the records illustrated in Fig. 3. The probability density functions for each record (thick lines) and for individual components (thin lines) were calculated with best-fit state models. Insets indicate time constants (τ) and fractional areas (a) for the illustrated exponential components.

scheme. However, given the kinetic multiplicity of open states observed and the necessarily limited experimental observations, we opted to represent each open level as a single state, with the understanding that the O and O_P states represent aggregates of several kinetically distinct classes. Previous work established that during activation in the absence of Ca^{2+}, three fully liganded closed states are accessed sequentially C_3-C_2-C_1 before the channel opens (Popescu and Auerbach, 2003; Popescu et al., 2004; Auerbach and Zhou, 2005; Zhang

TABLE 2

Kinetic components of single-channel closed events

$[Ca^{2+}]$	τ_{E1}	a_{E1}	τ_{E2}	a_{E2}	τ_{E3}	a_{E3}	τ_{E4}	a_{E4}	τ_{E5}	a_{E5}
mM	*ms*	%	*ms*	%	*ms*	%	*ms*	%	*ms*	%
0	0.20 ± 0.01	27 ± 2	2.4 ± 0.3	33 ± 5	6.9 ± 0.8	34 ± 4	24 ± 5	4.8 ± 2.0	3,300 ± 600	0.19 ± 0.07
1.8	0.52 ± 0.04[a]	40 ± 3[a]	2.9 ± 0.3	39 ± 3	7.2 ± 0.7	20 ± 5	240 ± 100[a]	1.19 ± 0.85[a]	6,000 ± 800[a]	0.19 ± 0.05
5	0.98 ± 0.24[a]	44 ± 8[a]	4.4 ± 0.4[a]	44 ± 5	26 ± 10	9.5 ± 3.7[a]	850 ± 360[a]	1.56 ± 0.59[a]	5,700 ± 900[a]	1.0 ± 0.4[a]
75	0.60 ± 0.07[a]	72 ± 6[a]	3.8 ± 0.5[a]	24 ± 5	23 ± 4[a]	2.1 ± 0.8[a]	1,300 ± 700[*]	0.58 ± 0.47[a]	19,000 ± 5,000[a]	0.96 ± 0.52[a]

[a]$P < 0.05$ relative to 0 mM Ca^{2+} (paired *t* test).

TABLE 3

Kinetic components of single-channel open events

$[Ca^{2+}]$	τ_{EF}	a_{EF}	τ_{EL}	a_{EL}	τ_{EM}	a_{EM}	τ_{EH}	a_{EH}
mM	*ms*	%	*ms*	%	*ms*	%	*ms*	%
0	0.29 ± 0.11	10 ± 0.8	2.3 ± 0.3	46 ± 11	5.0 ± 0.6	34 ± 8	11 ± 3	9.2 ± 4.0
1.8	0.33 ± 0.11	2.4 ± 0.4[a]	2.5 ± 0.4	37 ± 12	5.0 ± 0.6	48 ± 11	8.4 ± 1.0	12 ± 5
5	0.11	4.18	1.0	19	3.8 ± 0.5	58 ± 7[a]	7.1 ± 1.9	18 ± 10
75	-	-	-	-	5.2 ± 0.5	77 ± 6*	14 ± 3	23 ± 7

[a]$P < 0.05$ relative to 0 mM Ca^{2+} (paired *t* test).

et al., 2008); in addition, two desensitized states, C_4 and C_5, can be accessed from C_2 and C_3, respectively (Kussius et al., 2009). We fit several models to the single-channel records obtained in the presence of Ca^{2+} and ranked these according to their LL values. We found that data were best described by a model in which the overall arrangement of states was maintained with the following changes: the larger conductance O_P state substituted the O state, and an additional open state, O_S, was incorporated by forming a loop between O_P and C_1, the fastest closed state (Fig. 5 A). The rates optimized by fits to data obtained in 1.8 mM Ca^{2+} were slower within the activation sequence ($C_2 \rightarrow C_1 \rightarrow O_P$ and $C_2 \leftarrow C_1$) and were faster for entry into the main desensitized state ($C_3 \rightarrow C_5$) and slower for recovery ($C_5 \rightarrow C_3$). These changes in reaction mechanism predict that active receptors will drain into desensitized states at the expense of all other states, especially preopen closed states (Fig. 5 A, inset). The calculated energy landscapes illustrate that Ca^{2+} binding increased the stability of the principal desensitized state C_5 and slightly elevated energy barriers along the activation pathway (Fig. 5 B).

Given that Ca^{2+} inhibits channel gating with a half-maximal concentration of ~1.7 mM, the kinetic models describing channel gating patterns in the presence of physiological levels of Ca^{2+} likely represents a mean of gating rates for Ca^{2+}-free and Ca^{2+}-bound receptor states. To capture the concentration dependence of gating modulation by Ca^{2+}, we developed a tiered model with Ca^{2+}-free and Ca^{2+}-bound arms (Fig. 6 A). To limit the number of variables in this expanded model, within the Ca^{2+}-free arm we fixed all of the transitions rates to those experimentally determined in the absence of Ca^{2+}, and within the Ca^{2+}-bound arm we fixed those rates that were not significantly changed in 1.8 mM Ca^{2+} relative to 0 mM Ca^{2+} (Fig. 5 A). Next, to determine whether Ca^{2+} binding occurred preferentially to particular states, we connected the two arms with a single binding step whose position varied between models and evaluated the goodness of fit for each model based on an LL criterion (see Materials and methods). Only three models produced good fits, those with the binding step connecting (1) the C_2 states, (2) the C_1 states, or (3) the O and O_P states. Of these, the model connecting O with O_P produced the largest LL values. Notably, models that included a Ca^{2+}-binding step between the C_3, C_4, or C_5 states in each tier failed to converge on an acceptable fit. Importantly, this model implies that Ca^{2+}-bound receptors may occupy all closed states, even though association/dissociation occurs with observable probability only when receptors are actively gating (C_2, C_1,

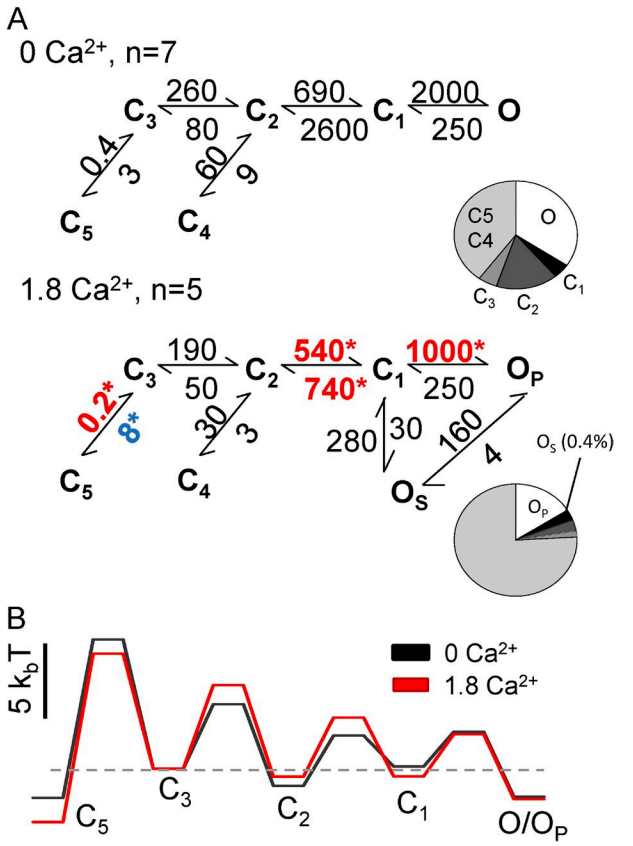

Figure 5. Effects of physiological $[Ca^{2+}]$ on reaction mechanisms. (A) State models (C, closed; O, open; O_P, principal open; O_S, secondary open) representing agonist bound states. Transition rates (s^{-1}) were optimized by fitting the model to one-channel cell-attached data (Fig. 4) and are given as rounded means for each dataset. Values that were statically slower (red) or faster (blue), relative to 0 mM Ca^{2+} (*, $P < 0.05$; unpaired *t* test) are highlighted. Pie charts illustrate predicted fractional occupancies for each state. (B) Free energy profiles calculated with the values in A represented relative to the C_3 states. C_4 and O_S states were omitted for clarity; all principal open states were aggregated as O or O_P for 0 and 1.8 mM Ca^{2+}, respectively.

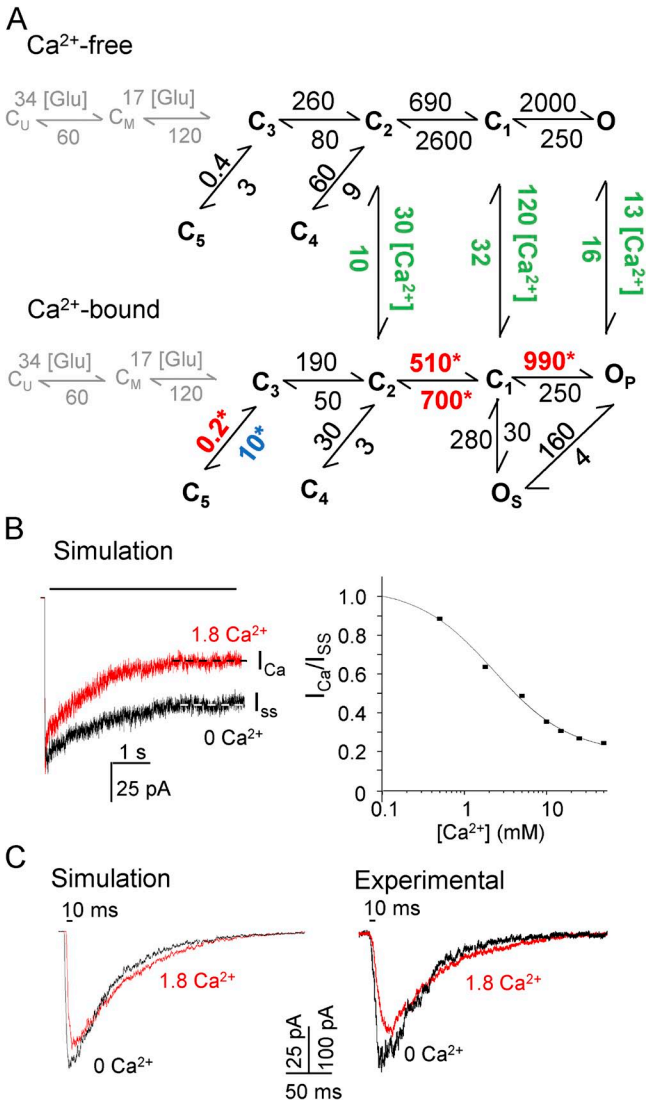

Figure 6. Effects of physiological [Ca^{2+}] on macroscopic responses. (A) Tiered state model represents Ca^{2+}-free (top) and Ca^{2+}-bound (bottom) arms. In gray are glutamate on ($\mu M^{-1}s^{-1}$) and off rates (s^{-1}), which were fixed to values measured previously (Popescu et al., 2004). In black are gating rates for the Ca^{2+}-free arm and those on the Ca^{2+}-bound arm that were unchanged in the presence of Ca^{2+}, which were fixed to the values indicated in Fig. 5 A. Ca^{2+} on rates ($M^{-1}s^{-1}$), off rates (s^{-1}), and variable gating transitions within the Ca^{2+}-bound arm were estimated by fitting the tiered model to single-channel records obtained in 1.8 mM Ca^{2+} ($n = 5$) and are given as rounded means. Asterisks indicate values that were significantly faster (blue) or slower (red) relative to their Ca^{2+}-free counterpart (*, $P < 0.05$; unpaired t test). (B, left) Simulated macroscopic responses (100 channels) to long (5 s) pulses of 1 mM glutamate using the model in A and the experimentally determined unitary conductances (Fig. 2) in the presence of 0 (black) or 1.8 mM Ca^{2+} (red). (right) Dose dependency of the I_{ss} levels of the simulated currents. (C, left) Macroscopic responses (100 channels) to brief pulses (10 ms) of 1 mM glutamate were simulated using the complete tiered model in A and the experimentally determined unitary conductances (Fig. 2) in the presence of 0 (black) or 1.8 mM Ca^{2+} (red). (right) Representative macroscopic responses to a 10-ms pulse of 1 mM glutamate recorded from an outside-out excised patch in the presence of 0 (black) or 1.8 mM Ca^{2+} (red).

and O). The Ca^{2+} dissociation constant calculated from microscopic association and dissociation rate constants ($K_d = k_-/k_+$) optimized with binding steps at C_2 and C_1 were similar (K_d = 0.3 mM); however, the model with the binding step between O and O_P predicted slightly lower Ca^{2+} affinity (K_d = 1.2 mM). These values match well with those previously determined (Premkumar and Auerbach, 1996; Sharma and Stevens, 1996).

As an immediate test for the tiered model, we simulated macroscopic responses (100 channels) in several external [Ca^{2+}], using the measured unitary conductances and the corresponding gating models. By fitting the Hill equation to the dose dependency of I_{Ca}/I_{ss}, we calculated maximal inhibition (~85%) and IC_{50} (2.3 ± 0.2 mM; Fig. 6 B). These values matched closely those determined experimentally with whole-cell recordings (Fig. 1 A), indicating that the model encapsulates the relevant features of Ca^{2+}-dependent effects on NMDA receptor responses. Considering that 1.8 mM Ca^{2+} produced a 15% reduction in conductance (Fig. 2) and a 30% reduction in gating (Fig. 3), these results, which correspond to a combined reduction current by ~40–45%, fully explain the inhibition observed in whole-cell currents (Fig. 1). Importantly our calculations imply that only approximately one third of the inhibition is caused by reduced conductance, with the largest proportion of the effect contributed by reduced gating, a phenomenon which has not been appreciated as of yet.

GluN1/GluN2A macroscopic responses in physiological [Ca^{2+}]

Aside from quantitative and mechanistic explanations for the observed changes in behavior, kinetic models are also valuable if they can predict the trajectory of the receptor response in a variety of conditions, some of which, although relevant to physiological and pathological conditions, may be difficult to achieve experimentally. We therefore examined whether the Ca^{2+} effects on conductance and gating captured in our model were sufficient to recapitulate receptor responses to stimuli likely to be experienced in situ. To address this, we examined macroscopic current responses to phasic stimulation. We simulated responses from 100 resting receptors after a brief (10 ms) exposure to 1 mM glutamate in the absence and presence of physiological levels (1.8 mM) of Ca^{2+}. Although slightly longer than a synaptic pulse, which was estimated to be ~1 ms (Clements et al., 1992), a 10-ms stimulus elicits NMDA receptor responses that are larger and less variable (Popescu et al., 2004), and thus easier to record reliably, but are sufficiently short to preclude any substantial entry into desensitized states (Zhang et al., 2008). To perform the simulation, we used the measured unitary conductances for each condition (Fig. 2) and the kinetic model illustrated in Fig. 6 A. The simulation predicted that relative to 0 mM Ca^{2+}, in 1.8 mM Ca^{2+} the peak response (I_{pk}) would decrease by ~10%; however,

the RT and time constant of deactivation would increase by ∼25 and ∼100%, respectively (Fig. 6 C). To test these predictions, we recorded macroscopic responses from outside-out patches after exposing them to glutamate (10 ms, 1 mM) using a fast piezo-driven perfusion system. Under both conditions, the decaying portion of the current trace was fit well by a double exponential function, consistent with the presence of modal gating (Zhang et al., 2008), which was not explicitly included in the tiered model used for simulations; therefore, for comparison, we determined the time course of decay as the weighted mean time constant (τ_w). We found that relative to 0 mM Ca^{2+}, 1.8 mM Ca^{2+} reduced peak current ∼20%, whereas RT and τ_w increased by ∼25 and ∼100%, respectively (Fig. 6 C and Table 4). Given that the rate constants in the model were optimized to cell-attached data, the close congruence between simulated traces and the responses measured from excised patches indicates that the tiered model, although only an approximation of the true reaction mechanism, captures the most relevant features of the direct effects of [Ca^{2+}] on NMDA receptor responses.

Importantly, the model highlights a consequential effect of fluctuations in external Ca^{2+} on the phasic response; it shows that although the peak current is indeed decreased by [Ca^{2+}], the deactivation time constant, which is a fundamental feature of the NMDA receptor response, increased. As a consequence, the overall charge transfer (calculated as the integrated current per time) increased from 58 to 90 fC per 100 channels. Therefore, our model predicts that transient fluctuations in external [Ca^{2+}] will influence both the amplitude and the time course of NMDA receptor responses.

DISCUSSION

We present here a quantitative description of the direct inhibitory effects of extracellular [Ca^{2+}] on GluN1/GluN2A channel conductance and gating kinetics and include predictions as to how this modulation may shape receptor responses to phasic and tonic stimulation patterns. We found that low millimolar levels of Ca^{2+} decreased whole-cell currents independently of the receptors' intracellular domains, and the mechanism included reductions in both channel conductance and channel activity. Furthermore, we developed a kinetic model that incorporates both of these effects and describes channel activity across the range of external Ca^{2+} concentrations typical of glutamatergic synapses. Relative to low Ca^{2+} conditions, our model predicts that 1.8 mM Ca^{2+} will almost double the charge transfer elicited by brief glutamate pulses (Fig. 6 C), but will substantially decrease the ionic flux during periods of chronic stimulation (Fig. 6 B). Importantly, because the K_d we estimated for Ca^{2+} (1.2 mM) was in the physiological range, we anticipate that local fluctuations in extracellular Ca^{2+} will influence the amplitude and time course of NMDA receptor responses in situ. Notably, synchronous activities in large populations of neurons or bouts of intense synaptic firing are likely to change the ionic composition of the extracellular space, in particular by decreasing Ca^{2+}. Consequently, under normal conditions, the signal generated by NMDA receptors may vary on a rapid timescale as the availability for Ca^{2+} to modulate channel properties fluctuates.

Our observation that the [Ca^{2+}]-dependent reduction in current was independent of the receptors' intracellular domains indicates that the inhibition was mediated by direct interactions between Ca^{2+} ions and receptor residues. These results were unexpected as the current literature on inhibition of NMDA receptor gating by Ca^{2+} speaks exclusively to indirect mechanisms, even though these may represent modulatory layers that operate on longer time scales or may be preparation specific (Rosenmund and Westbrook, 1993; Zhang et al., 1998; Krupp et al., 1999). Importantly, the [Ca^{2+}]-dependent reduction in current was intact at depolarized potentials, indicating that the Ca^{2+}-binding site responsible for this direct inhibition is located outside the membrane (Woodhull, 1973), and therefore, the inhibition is more likely to occur through an allosteric rather than a channel block mechanism.

Direct interactions between Ca^{2+} ions and charged residues outside of the voltage field produce a reduction in channel conductance that is well documented in the literature (Ascher and Nowak, 1988; Jahr and Stevens, 1993; Watanabe et al., 2002). Here, we observed a 76 ± 4% maximal reduction in conductance of the principal open level, γ_P, for channels contained in excised patches as well as the emergence of a prominent secondary conductance level, γ_S, with increasing concentrations of external Ca^{2+}. Increasing [Ca^{2+}] lowered both the P and S levels with similar potencies (IC_{50} = 6.3 ± 0.8 and 6.4 ± 1.0 mM for γ_P and γ_S, respectively). Both of these values are slightly higher than the estimates in a previous study (K_d = ∼1 mM); this may be primarily the result of the very low [Ca^{2+}] range (10 nm to 10 mM) used in the previous study, whose goal was to characterize a higher-affinity Ca^{2+}-binding site (Premkumar and Auerbach, 1996).

Although the [Ca^{2+}]-dependent reduction was similar for both conductance levels, the Hill coefficients were

TABLE 4

Effects of external [Ca^{2+}] on macroscopic activation and deactivation kinetics

[Ca^{2+}]	I_{pk}	RT	τ_w
mM	*pA*	*ms*	*ms*
0	170 ± 50	4.4 ± 0.8	39 ± 5
1.8	130 ± 40	5.7 ± 1.1[a]	59 ± 5[a]

[a]$P < 0.05$ relative to 0 mM Ca^{2+} (paired *t* test).

clearly different: ~1 and ~2.5 for γ_P and γ_S, respectively. This observation may indicate that two or more Ca^{2+}-binding sites are cooperative when the channel is in O_S but not in O_P states; how this happens, however, is unclear. The current literature indicates that mutation of the channel's Mg^{2+}-blocking site, which resides deep within the membrane pore on GluN2A subunits, increases the binding affinity of Ca^{2+} to its external binding site (Premkumar and Auerbach, 1996; Sharma and Stevens, 1996). Furthermore, mutations of the homologous residues in the GluN1 subunit produce a prominent subconductance level in the absence of Ca^{2+} (Premkumar and Auerbach, 1996; Premkumar et al., 1997). Based on these observations and our finding that increasing the concentration of external Ca^{2+} increases the probability of O_S states, it is possible that small structural perturbations in the channel's pore region, resulting from Ca^{2+} permeation, could alter the structure of the external vestibule, leading to stronger Ca^{2+} binding at that site and subsequently lower channel conductance.

In addition to changes in conductance, we discovered that $[Ca^{2+}]$ also altered the NMDA receptor gating reaction. To approximate channel kinetics in physiological $[Ca^{2+}]$, an additional open state, O_S, corresponding to the secondary conductance level, S, was added into the model, and this was best incorporated by forming a loop with the C_1 closed state and the principal open state, O_P. Within this reaction mechanism, several transitions were sensitive to $[Ca^{2+}]$: transitions between preopen closed states were slowed, entry into desensitization was accelerated, and resensitization was slowed. Additionally, high concentrations of Ca^{2+} abolished the very brief openings. These findings are valuable given that neither the structural correlates for individual kinetic states nor the mechanisms for desensitization are known (Borschel et al., 2011), and possibly structural information regarding Ca^{2+}-receptor interactions can help elucidate the molecular mechanisms behind these phenomena. We note that although we measured IC_{50} values for Ca^{2+} in the low millimolar range for both conductance and gating effects, we cannot determine whether these are mediated by the same or different sites.

The kinetic scheme we generated represents a valuable tool to predict the signal generated by NMDA receptors in response to various physiological stimuli across the range of external Ca^{2+} levels that occurs during normal and pathological conditions. Models that have been previously generated in the presence of Ca^{2+} have assumed a fixed external $[Ca^{2+}]$ and do not distinguish gating differences between Ca^{2+}-free and Ca^{2+}-bound receptors (Banke and Traynelis, 2003; Schorge et al., 2005). Therefore, the rates estimated with these models represent a mean of transition rates of Ca^{2+}-bound and Ca^{2+}-free receptors. Because the extent to which a receptor dwells in a Ca^{2+}-bound or Ca^{2+}-free state will vary substantially based on changes in external $[Ca^{2+}]$, predicted macroscopic responses based on such models can only be applied to a static condition. The model developed here bypasses this limitation and allows for sensitive changes in NMDA receptor response according to the rapid dynamics of extracellular Ca^{2+} levels to be accurately inferred.

With this model, simulations of ensemble responses to brief and prolonged pulses of glutamate predicted that the external Ca^{2+} concentration effectively shapes the NMDA receptor response. Specifically, in response to a single, brief exposure to glutamate, Ca^{2+} ions slowed both the activation and deactivation kinetics and increased substantially the charge transferred during a single activation. In contrast, Ca^{2+} ions deepened the receptor desensitization and reduced the overall flux during extended exposures to glutamate. This stimulus-dependent effect of Ca^{2+} on charge transfer may play important roles in neuronal physiology.

The distinct intracellular milieu of synaptic and extrasynaptic NMDA receptors controls the cellular effect of the Ca^{2+} influx such that activation of synaptic receptors generally promotes cell survival and synaptic plasticity, whereas activation of extrasynaptic receptors can initiate apoptotic cascades (Hardingham and Bading, 2010). Given that synaptic and extrasynaptic receptors experience fundamentally distinct glutamate transients, our result that fluctuations in external Ca^{2+} have opposing effects on the charge transferred in response to phasic and tonic stimulation adds another layer to the distinct roles played by NMDA receptors at synaptic versus extrasynaptic locations. Therefore, the quantitative description provided here will help to further elucidate the role of fluctuating external $[Ca^{2+}]$ in health and disease.

We thank Dr. Gary Westbrook (Vollum Institute, Oregon Health and Science University, Portland, OR) for providing NMDA receptor constructs lacking intracellular domains and Ms. Eileen Kasperek for assistance with cell culture, media preparation, and molecular biology.

This work was supported in part by the National Institutes of Health (RO1 NS052669), the American Heart Association Established Investigator Award (AHA 12EIA9100012), and the SUNY REACH initiative.

The authors declare no competing financial interests.

Kenton J. Swartz served as editor.

Submitted: 13 June 2014
Accepted: 29 September 2014

REFERENCES

Amico-Ruvio, S.A., S.E. Murthy, T.P. Smith, and G.K. Popescu. 2011. Zinc effects on NMDA receptor gating kinetics. *Biophys. J.* 100:1910–1918. http://dx.doi.org/10.1016/j.bpj.2011.02.042

Ascher, P., and L. Nowak. 1988. The role of divalent cations in the *N*-methyl-D-aspartate responses of mouse central neurones in culture. *J. Physiol.* 399:247–266.

Auerbach, A., and Y. Zhou. 2005. Gating reaction mechanisms for NMDA receptor channels. *J. Neurosci.* 25:7914–7923. http://dx.doi.org/10.1523/JNEUROSCI.1471-05.2005

Banke, T.G., and S.F. Traynelis. 2003. Activation of NR1/NR2B NMDA receptors. *Nat. Neurosci.* 6:144–152. http://dx.doi.org/10.1038/nn1000

Banke, T.G., S.M. Dravid, and S.F. Traynelis. 2005. Protons trap NR1/NR2B NMDA receptors in a nonconducting state. *J. Neurosci.* 25:42–51. http://dx.doi.org/10.1523/JNEUROSCI.3154-04.2005

Benninger, C., J. Kadis, and D.A. Prince. 1980. Extracellular calcium and potassium changes in hippocampal slices. *Brain Res.* 187: 165–182. http://dx.doi.org/10.1016/0006-8993(80)90502-8

Borschel, W.F., S.E. Murthy, E.M. Kasperek, and G.K. Popescu. 2011. NMDA receptor activation requires remodelling of intersubunit contacts within ligand-binding heterodimers. *Nat. Commun.* 2:498. http://dx.doi.org/10.1038/ncomms1512

Burnashev, N., R. Schoepfer, H. Monyer, J.P. Ruppersberg, W. Günther, P.H. Seeburg, and B. Sakmann. 1992. Control by asparagine residues of calcium permeability and magnesium blockade in the NMDA receptor. *Science.* 257:1415–1419. http://dx.doi.org/10.1126/science.1382314

Burnashev, N., Z. Zhou, E. Neher, and B. Sakmann. 1995. Fractional calcium currents through recombinant GluR channels of the NMDA, AMPA and kainate receptor subtypes. *J. Physiol.* 485:403–418.

Chen, B.S., and K.W. Roche. 2007. Regulation of NMDA receptors by phosphorylation. *Neuropharmacology.* 53:362–368. http://dx.doi.org/10.1016/j.neuropharm.2007.05.018

Chen, C., and H. Okayama. 1987. High-efficiency transformation of mammalian cells by plasmid DNA. *Mol. Cell. Biol.* 7:2745–2752.

Choi, U.B., S. Xiao, L.P. Wollmuth, and M.E. Bowen. 2011. Effect of Src kinase phosphorylation on disordered C-terminal domain of *N*-methyl-D-aspartic acid (NMDA) receptor subunit GluN2B protein. *J. Biol. Chem.* 286:29904–29912. http://dx.doi.org/10.1074/jbc.M111.258897

Christine, C.W., and D.W. Choi. 1990. Effect of zinc on NMDA receptor-mediated channel currents in cortical neurons. *J. Neurosci.* 10:108–116.

Clements, J.D., R.A. Lester, G. Tong, C.E. Jahr, and G.L. Westbrook. 1992. The time course of glutamate in the synaptic cleft. *Science.* 258:1498–1501. http://dx.doi.org/10.1126/science.1359647

Colquhoun, D., and A.G. Hawkes. 1995. The principles of the stochastic interpretation of ion-channel mechanisms. *In* Single-Channel Recording. B. Sakmann and E. Neher, editors. Springer US, New York. 397–482.

Dravid, S.M., A. Prakash, and S.F. Traynelis. 2008. Activation of recombinant NR1/NR2C NMDA receptors. *J. Physiol.* 586: 4425–4439. http://dx.doi.org/10.1113/jphysiol.2008.158634

Erreger, K., and S.F. Traynelis. 2008. Zinc inhibition of rat NR1/NR2A *N*-methyl-D-aspartate receptors. *J. Physiol.* 586:763–778. http://dx.doi.org/10.1113/jphysiol.2007.143941

Erreger, K., S.M. Dravid, T.G. Banke, D.J.A. Wyllie, and S.F. Traynelis. 2005. Subunit-specific gating controls rat NR1/NR2A and NR1/NR2B NMDA channel kinetics and synaptic signalling profiles. *J. Physiol.* 563:345–358. http://dx.doi.org/10.1113/jphysiol.2004.080028

Hardingham, G.E., and H. Bading. 2010. Synaptic versus extrasynaptic NMDA receptor signalling: implications for neurodegenerative disorders. *Nat. Rev. Neurosci.* 11:682–696. http://dx.doi.org/10.1038/nrn2911

Heinemann, U., and R. Pumain. 1980. Extracellular calcium activity changes in cat sensorimotor cortex induced by iontophoretic application of aminoacids. *Exp. Brain Res.* 40:247–250. http://dx.doi.org/10.1007/BF00237788

Heinemann, U., A. Konnerth, R. Pumain, and W.J. Wadman. 1986. Extracellular calcium and potassium concentration changes in chronic epileptic brain tissue. *Adv. Neurol.* 44:641–661.

Jahr, C.E., and C.F. Stevens. 1993. Calcium permeability of the *N*-methyl-D-aspartate receptor channel in hippocampal neurons in culture. *Proc. Natl. Acad. Sci. USA.* 90:11573–11577. http://dx.doi.org/10.1073/pnas.90.24.11573

Johnson, J.W., and P. Ascher. 1987. Glycine potentiates the NMDA response in cultured mouse brain neurons. *Nature.* 325:529–531. http://dx.doi.org/10.1038/325529a0

Karakas, E., and H. Furukawa. 2014. Crystal structure of a heterotetrameric NMDA receptor ion channel. *Science.* 344:992–997. http://dx.doi.org/10.1126/science.1251915

Kleckner, N.W., and R. Dingledine. 1988. Requirement for glycine in activation of NMDA-receptors expressed in Xenopus oocytes. *Science.* 241:835–837. http://dx.doi.org/10.1126/science.2841759

Krupp, J.J., B. Vissel, C.G. Thomas, S.F. Heinemann, and G.L. Westbrook. 1999. Interactions of calmodulin and α-actinin with the NR1 subunit modulate Ca^{2+}-dependent inactivation of NMDA receptors. *J. Neurosci.* 19:1165–1178.

Krupp, J.J., B. Vissel, C.G. Thomas, S.F. Heinemann, and G.L. Westbrook. 2002. Calcineurin acts via the C-terminus of NR2A to modulate desensitization of NMDA receptors. *Neuropharmacology.* 42:593–602. http://dx.doi.org/10.1016/S0028-3908(02)00031-X

Kuner, T., L.P. Wollmuth, A. Karlin, P.H. Seeburg, and B. Sakmann. 1996. Structure of the NMDA receptor channel M2 segment inferred from the accessibility of substituted cysteines. *Neuron.* 17:343–352. http://dx.doi.org/10.1016/S0896-6273(00)80165-8

Kussius, C.L., N. Kaur, and G.K. Popescu. 2009. Pregnanolone sulfate promotes desensitization of activated NMDA receptors. *J. Neurosci.* 29:6819–6827. http://dx.doi.org/10.1523/JNEUROSCI.0281-09.2009

Lee, C.-H., W. Lü, J.C. Michel, A. Goehring, J. Du, X. Song, and E. Gouaux. 2014. NMDA receptor structures reveal subunit arrangement and pore architecture. *Nature.* 511:191–197. http://dx.doi.org/10.1038/nature13548

Legendre, P., and G.L. Westbrook. 1990. The inhibition of single *N*-methyl-D-aspartate-activated channels by zinc ions on cultured rat neurones. *J. Physiol.* 429:429–449.

Lester, R.A., and C.E. Jahr. 1992. NMDA channel behavior depends on agonist affinity. *J. Neurosci.* 12:635–643.

Magleby, K.L., and B.S. Pallotta. 1983. Burst kinetics of single calcium-activated potassium channels in cultured rat muscle. *J. Physiol.* 344:605–623.

Maki, B.A., T.K. Aman, S.A. Amico-Ruvio, C.L. Kussius, and G.K. Popescu. 2012. C-terminal domains of *N*-methyl-D-aspartic acid receptor modulate unitary channel conductance and gating. *J. Biol. Chem.* 287:36071–36080. http://dx.doi.org/10.1074/jbc.M112.390013

Mayer, M.L., and G.L. Westbrook. 1987. Permeation and block of *N*-methyl-D-aspartic acid receptor channels by divalent cations in mouse cultured central neurones. *J. Physiol.* 394:501–527.

Mayer, M.L., G.L. Westbrook, and P.B. Guthrie. 1984. Voltage-dependent block by Mg^{2+} of NMDA responses in spinal cord neurones. *Nature.* 309:261–263. http://dx.doi.org/10.1038/309261a0

Monyer, H., N. Burnashev, D.J. Laurie, B. Sakmann, and P.H. Seeburg. 1994. Developmental and regional expression in the rat brain and functional properties of four NMDA receptors. *Neuron.* 12:529–540. http://dx.doi.org/10.1016/0896-6273(94)90210-0

Neher, E., and J.H. Steinbach. 1978. Local anaesthetics transiently block currents through single acetylcholine-receptor channels. *J. Physiol.* 277:153–176.

Nicholson, C., G.T. Bruggencate, R. Steinberg, and H. Stöckle. 1977. Calcium modulation in brain extracellular microenvironment demonstrated with ion-selective micropipette. *Proc. Natl. Acad. Sci. USA.* 74:1287–1290. http://dx.doi.org/10.1073/pnas.74.3.1287

Nowak, L., P. Bregestovski, P. Ascher, A. Herbet, and A. Prochiantz. 1984. Magnesium gates glutamate-activated channels in mouse central neurones. *Nature.* 307:462–465. http://dx.doi.org/10.1038/307462a0

Paoletti, P., P. Ascher, and J. Neyton. 1997. High-affinity zinc inhibition of NMDA NR1-NR2A receptors. *J. Neurosci.* 17:5711–5725.

Pearce, S.H., and R.V. Thakker. 1997. The calcium-sensing receptor: insights into extracellular calcium homeostasis in health and disease. *J. Endocrinol.* 154:371–378. http://dx.doi.org/10.1677/joe.0.1540371

Popescu, G., and A. Auerbach. 2003. Modal gating of NMDA receptors and the shape of their synaptic response. *Nat. Neurosci.* 6:476–483.

Popescu, G., A. Robert, J.R. Howe, and A. Auerbach. 2004. Reaction mechanism determines NMDA receptor response to repetitive stimulation. *Nature.* 430:790–793. http://dx.doi.org/10.1038/nature02775

Premkumar, L.S., and A. Auerbach. 1996. Identification of a high affinity divalent cation binding site near the entrance of the NMDA receptor channel. *Neuron.* 16:869–880. http://dx.doi.org/10.1016/S0896-6273(00)80107-5

Premkumar, L.S., F. Qin, and A. Auerbach. 1997. Subconductance states of a mutant NMDA receptor channel kinetics, calcium, and voltage dependence. *J. Gen. Physiol.* 109:181–189. http://dx.doi.org/10.1085/jgp.109.2.181

Qin, F. 2004. Restoration of single-channel currents using the segmental k-means method based on hidden Markov modeling. *Biophys. J.* 86:1488–1501. http://dx.doi.org/10.1016/S0006-3495(04)74217-4

Qin, F., A. Auerbach, and F. Sachs. 1997. Maximum likelihood estimation of aggregated Markov processes. *Proc. Biol. Sci.* 264:375–383. http://dx.doi.org/10.1098/rspb.1997.0054

Rosenmund, C., and G.L. Westbrook. 1993. Calcium-induced actin depolymerization reduces NMDA channel activity. *Neuron.* 10:805–814. http://dx.doi.org/10.1016/0896-6273(93)90197-Y

Rusakov, D.A., and A. Fine. 2003. Extracellular Ca^{2+} depletion contributes to fast activity-dependent modulation of synaptic transmission in the brain. *Neuron.* 37:287–297. http://dx.doi.org/10.1016/S0896-6273(03)00025-4

Rycroft, B.K., and A.J. Gibb. 2004a. Inhibitory interactions of calcineurin (phosphatase 2B) and calmodulin on rat hippocampal NMDA receptors. *Neuropharmacology.* 47:505–514. http://dx.doi.org/10.1016/j.neuropharm.2004.06.001

Rycroft, B.K., and A.J. Gibb. 2004b. Regulation of single NMDA receptor channel activity by alpha-actinin and calmodulin in rat hippocampal granule cells. *J. Physiol.* 557:795–808. http://dx.doi.org/10.1113/jphysiol.2003.059212

Schorge, S., S. Elenes, and D. Colquhoun. 2005. Maximum likelihood fitting of single channel NMDA activity with a mechanism composed of independent dimers of subunits. *J. Physiol.* 569:395–418. http://dx.doi.org/10.1113/jphysiol.2005.095349

Sharma, G., and C.F. Stevens. 1996. Interactions between two divalent ion binding sites in *N*-methyl-D-aspartate receptor channels. *Proc. Natl. Acad. Sci. USA.* 93:14170–14175. http://dx.doi.org/10.1073/pnas.93.24.14170

Silver, I.A., and M. Erecińska. 1990. Intracellular and extracellular changes of $[Ca^{2+}]$ in hypoxia and ischemia in rat brain in vivo. *J. Gen. Physiol.* 95:837–866. http://dx.doi.org/10.1085/jgp.95.5.837

Tang, C.M., M. Dichter, and M. Morad. 1990. Modulation of the *N*-methyl-D-aspartate channel by extracellular H^+. *Proc. Natl. Acad. Sci. USA.* 87:6445–6449. http://dx.doi.org/10.1073/pnas.87.16.6445

Tong, G., D. Shepherd, and C.E. Jahr. 1995. Synaptic desensitization of NMDA receptors by calcineurin. *Science.* 267:1510–1512. http://dx.doi.org/10.1126/science.7878472

Traynelis, S.F., and S.G. Cull-Candy. 1990. Proton inhibition of *N*-methyl-D-aspartate receptors in cerebellar neurons. *Nature.* 345:347–350. http://dx.doi.org/10.1038/345347a0

Vance, K.M., K.B. Hansen, and S.F. Traynelis. 2013. Modal gating of GluN1/GluN2D NMDA receptors. *Neuropharmacology.* 71:184–190. http://dx.doi.org/10.1016/j.neuropharm.2013.03.018

Watanabe, J., C. Beck, T. Kuner, L.S. Premkumar, and L.P. Wollmuth. 2002. DRPEER: a motif in the extracellular vestibule conferring high Ca^{2+} flux rates in NMDA receptor channels. *J. Neurosci.* 22:10209–10216.

Wo, Z.G., and R.E. Oswald. 1995. Unraveling the modular design of glutamate-gated ion channels. *Trends Neurosci.* 18:161–168. http://dx.doi.org/10.1016/0166-2236(95)93895-5

Woodhull, A.M. 1973. Ionic blockage of sodium channels in nerve. *J. Gen. Physiol.* 61:687–708. http://dx.doi.org/10.1085/jgp.61.6.687

Zhang, S., M.D. Ehlers, J.P. Bernhardt, C.-T. Su, and R.L. Huganir. 1998. Calmodulin mediates calcium-dependent inactivation of *N*-methyl-D-aspartate receptors. *Neuron.* 21:443–453. http://dx.doi.org/10.1016/S0896-6273(00)80553-X

Zhang, W., J.R. Howe, and G.K. Popescu. 2008. Distinct gating modes determine the biphasic relaxation of NMDA receptor currents. *Nat. Neurosci.* 11:1373–1375. http://dx.doi.org/10.1038/nn.2214